Reduction of Base Drag by Boat-Tailed Afterbodies in Low-Speed Flow

W. A. MAIR

(Engineering Department, Cambridge University)

Summary: Drag measurements were made on a blunt-based body of revolution with the addition of several alternative boat-tailed afterbodies. The best of these afterbodies, with a length of only 60 per cent of the maximum diameter, gave almost as much reduction of drag as a conventional streamline tail. The pressure distribution on this body was measured for various lengths. It does not seem to be possible at present to predict quantitatively the drag of this type of body but some qualitative design principles have been suggested.

1. Introduction

Referring to Fig. 1, it has been known for many years that in low-speed flow the drag of a blunt-based body of revolution such as ABCFG may be reduced by the addition of a boat-tailed afterbody such as CDEF. There is a lack of information, however, on the optimum design of such an afterbody and the possible extent of the drag reduction. Moreover, in much of the previous work, the emphasis has been on the pressure coefficient C_{pB} at the base DE of the afterbody, and on the relationship between C_{pB} and the boat-tail angle θ, whereas the reduction of drag due to the afterbody may be expected to depend as much on the presssure distribution over the curved surface CD as on the base pressure.

In the present work the emphasis is on shapes of afterbody which are relatively short and yet give large reductions of drag. Some attempt is made to understand the factors on which the drag reduction depends and its probable upper limit.

Notation

$C_D = D/(\frac{1}{2}\rho U^2 \pi R^2)$, drag coefficient

ΔC_D reduction of drag coefficient due to addition of afterbody

C_{DB} base drag coefficient (based on area πR^2)

C_{DC} component of drag coefficient due to normal pressure on curved surface of afterbody

C_{Df} component of drag coefficient due to skin friction on afterbody

$C_p = (p - p_1)/\frac{1}{2}\rho U^2$, pressure coefficient

C_{pB} mean value of C_p over base

D drag

L = (length of afterbody)/R

Received January 1969.

[The Aeronautical Quarterly, Vol. XX, November 1969]

p pressure

p_1 pressure in undisturbed stream

R maximum radius of body

r=(radius of body)/R

U velocity of undisturbed stream

x=(axial distance from upstream end of afterbody)/R

θ boat-tail angle (*see* Fig. 1)

ρ air density

2. Drag Measurements

The model used for all the measurements was as shown in Fig. 1, with maximum radius $R=76$ mm. The nose portion ABG was ellipsoidal and various alternative afterbodies CDEF were used. A transition wire of diameter 0·46 mm was fixed 16 mm ahead of the joint BG and the thickness of the (turbulent) boundary layer at the station CF was then about 10 mm. All the measurements were repeated with the boundary layer thickened artificially by means of a thick rubber ring just ahead of the transition wire. Two thicknesses of ring were used, 3 and 6 mm, giving boundary-layer thicknesses of about 20 and 30 mm at CF, but unless otherwise stated all the results given here refer to the model with the thinnest (10 mm) boundary layer.

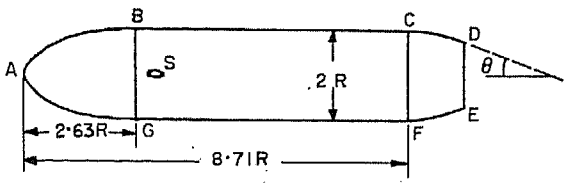

Figure 1. Body of revolution.

To support the model in the wind tunnel a horizontal streamline tube of chord 30 mm and thickness 11·5 mm was passed through the model at S. This tube was of total span 610 mm and was supported from the overhead balance by a pair of inclined wires at each end. To complete the support system a single vertical wire was attached to a point on the top of the model 28 mm upstream of C. All the wires were of diameter 0·7 mm.

The model was mounted at zero incidence in a closed wind tunnel with a working section 1·22 m high and 1·68 m wide. The wind speed was about 45 m/s, giving a Reynolds number of $0{\cdot}46 \times 10^6$ based on the maximum diameter of the body. Earlier work by Calvert[1] and by the author[2] has shown that for a model of this shape the method of Evans[3] gives a satisfactory estimate of the blockage correction and this method has been used for correcting all the measurements.

Basing the drag coefficient C_D on the area πR^2, attention was concentrated on the reduction of drag coefficient ΔC_D due to adding an afterbody to the basic model cut off at CF. The base drag coefficient for the basic model was found from the measured base pressure at CF, but the total drag coefficient of the model was not required and hence there was no need to estimate the drag of the supporting system.

Measurements over a small range of incidence with the basic model and with a selection of afterbodies showed no appreciable change of base pressure or drag over the range ± 2 deg. Thus small departures from the nominal zero incidence would have no effect on the measurements.

An ideal afterbody, with zero skin friction and with presssure distribution as for inviscid flow, would give $\Delta C_D \simeq -C_{pB}$, where C_{pB} is the mean base pressure coefficient for the basic model cut off at CF. For the basic model the flow in the region of the base was unsteady, so that it was difficult to measure $-C_{pB}$ accurately. The mean value was found to be about 0·165, in agreement with earlier measurements by Calvert[1] on the same model, but it should be noted that the possible error in this measurement is about $\pm 0{\cdot}005$.

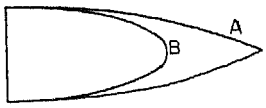

Figure 2. Conventional rear fairings.

To provide a standard of comparison for the boat-tailed afterbodies, drag measurements were made on the two conventional rear fairings shown in Fig. 2. Fairing A was obtained by scaling the "Body A" tested by Lock and Johansen[4] to give a fineness ratio of 4 and then taking the rear 2/3 of this body (aft of the maximum diameter). This gave a tail fairing with length equal to 2·67 times the maximum diameter. Fairing B was a semi-ellipsoid with length equal to 1·67 times the maximum diameter, this being close to the fineness ratio found by Wieghardt[5] to give minimum drag. The values of ΔC_D found for fairings A and B were respectively 0·118 and 0·119. Thus the addition of either of these fairings to the basic model reduced the base drag by about 72 per cent.

Drag measurements were made on eight boat-tailed afterbodies, as shown in Table I. In this table and in all the results to follow, all length dimensions are expressed as multiples of the maximum body radius. Each afterbody was constructed with plywood segments bolted and dowelled together, so that the length could be adjusted by varying the number of segments. The afterbodies were turned in a lathe after bolting the segments together and the maximum roughness height was only about 0·03 mm.

TABLE I

BOAT-TAILED AFTERBODIES

All lengths are expressed as multiples of the maximum body radius R.

r is the radius at an axial distance x from the upstream end of the afterbody (section CF in Fig. 1).

Body No.	*Description*
1	Ellipse, semi-major axis=1.67
2	Cubic, $r=1-0.168x^3$
3	Quartic, $r=1-0.319x^3+0.1185x^4$
4	Ellipse, semi-major axis=1.54
5	Quartic $r=1-0.405x^3+0.168x^4$
6	Sine curve of unit length, followed by cone of semi-angle 22 deg
7	Sine curve of unit length, followed by cone of semi-angle 26 deg
8	Sine curve of unit length, followed by cone of semi-angle 30 deg

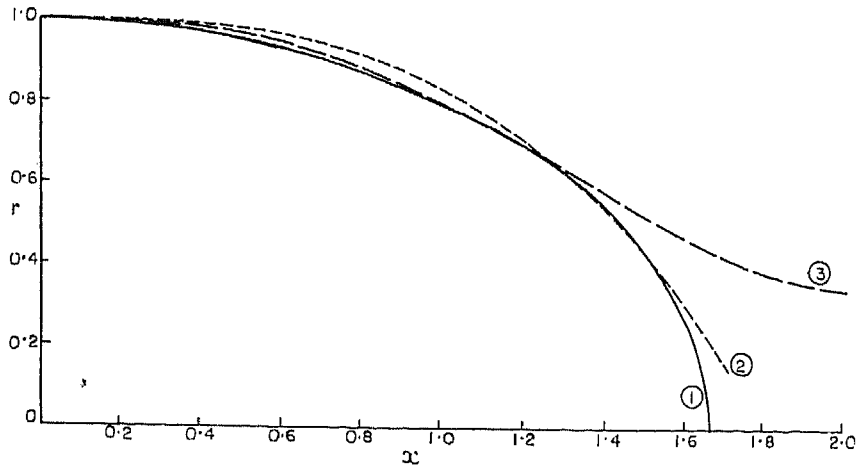

Figure 3. Boat-tailed afterbodies 1, 2 and 3.

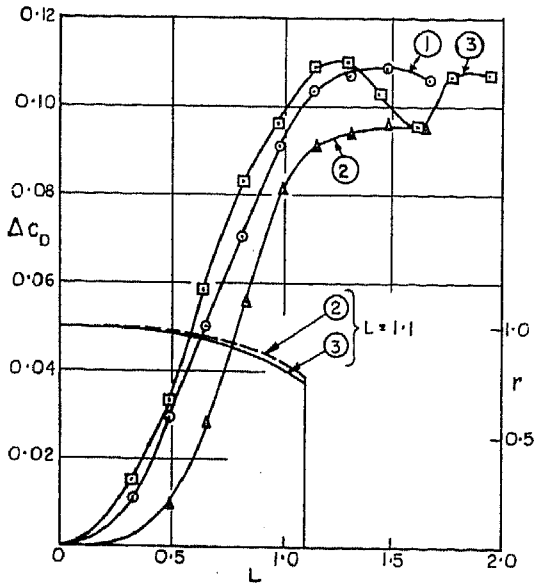

Figure 4. Drag reduction due to boat-tailed afterbodies 1, 2 and 3.

The design of the first three afterbodies of Table I was based on some earlier unpublished experiments in this laboratory by A. P. W. Martin and D. B. Rogers, using a smaller model. In these experiments circular-arc generators were used for the afterbodies and it was found that a good reduction of drag was obtained with a fairly short afterbody when the radius of the circular arc was in the region of 2·5 times the maximum body radius.

Figure 3 shows the afterbodies 1, 2 and 3 and Fig. 4 shows the values of ΔC_D plotted against the length L. Either of the afterbodies 1 and 3 is significantly better than 2 and gives a reduction of C_D exceeding 0·1 for an afterbody length not much greater than 1.

The double peak shown in Fig. 4 for body 3 is probably associated with variation of the position of separation. For $L \simeq 1{\cdot}6$ the drag fluctuated considerably

and separation was probably then occurring intermittently ahead of the cut-off base. For $L \simeq 1{\cdot}3$ and again for $L \simeq 1{\cdot}8$ there was no indication of unsteadiness in the measured drag. It seems likely that in both these cases separation was occurring close to the cut-off base, although for $L \simeq 1{\cdot}8$ there may have been a separation bubble further upstream. A similar double maximum of ΔC_D was found with some of the other bodies, sometimes only when the boundary layer was thickened, but always with noticeably unsteady flow in the region of the minimum ΔC_D. It seems clear that afterbodies behaving in this way should be avoided for practical use, although there should be no objection to the use of body 3, for example, with $L < 1{\cdot}3$.

Figure 4 suggests that for bodies 1 and 2 separation may occur ahead of the cut-off base for values of L greater than about 1·2 or 1·3, but the absence of severe drag fluctuations indicates that on these bodies the position of separation is nearly stationary.

The design of the bodies 1 and 3 was based on a circular arc of radius 2·5, the profiles being closely similar to the circular arc over the important range of x between about 0·9 and 1·3. It seemed possible that a drag reduction similar to that found for these bodies could be obtained with a shorter length by basing the design on a circular arc of smaller radius. Bodies 4 and 5 were therefore based on a circular arc of radius 2·17, their profiles agreeing closely with the circular arc in the range of x from about 0·8 to 1·2. The drag measurements on these bodies showed no significant change in the maximum value of ΔC_D, but the values of L on the steeply rising part of the curve were reduced by about 20 per cent in changing from body 1 to body 4 and by about 9 per cent from body 3 to body 5.

For all the shapes of afterbody considered so far, ΔC_D increases rapidly with L up to a certain value, but further increase of L gives little or no increase of ΔC_D. It is to be expected that, in order to achieve a large ΔC_D with a short afterbody, the boat-tail angle θ (as defined in Fig. 1) should be made as large as possible without causing separation ahead of the base. To give some indication of the optimum value of θ the results for bodies 1 to 5 were considered and the values of θ were found for lengths giving ΔC_D equal to 90 per cent of the maximum value. These values of θ are given in Table II; they all lie within a narrow range around 25 to 26 degrees except for body 2 which is known to be less satisfactory than the others.

TABLE II

BOAT-TAIL ANGLES θ FOR $\Delta C_D = 0{\cdot}9\Delta C_{D\max}$

Body No.	1	2	3	4	5
θ (degrees)	26·0	29·9	25·9	24·7	25·9

These results suggested that a conical afterbody with a semi-apex angle of about 26 degrees might be expected to give a good reduction of drag for a short length. Some form of smooth fairing is needed, of course, between the cylindrical body and the conical part of the afterbody and for this a sine curve of unit length was chosen, giving continuous slope and curvature at each end. It is not claimed that this form of fairing is necessarily the best, but the results obtained indicate that small variations in the shape of the fairing do not have any important effect on ΔC_D.

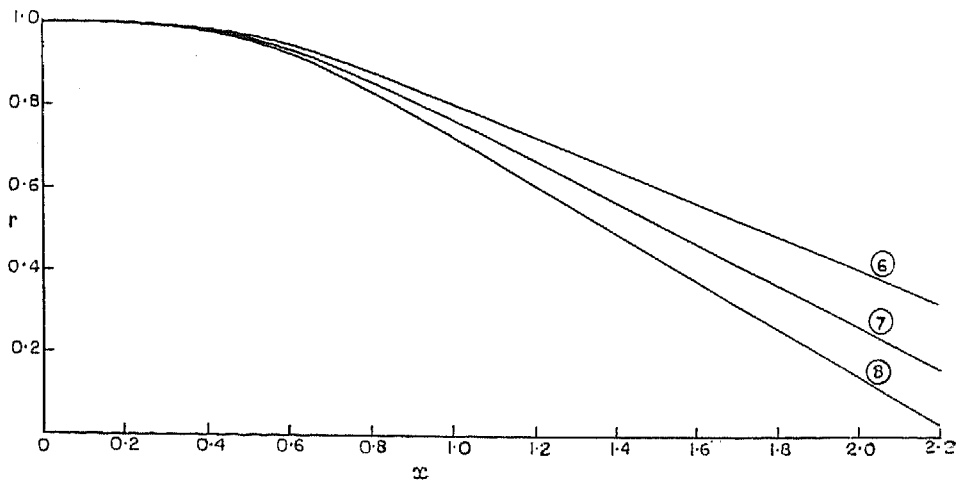

Figure 5. Boat-tailed afterbodies 6, 7 and 8.

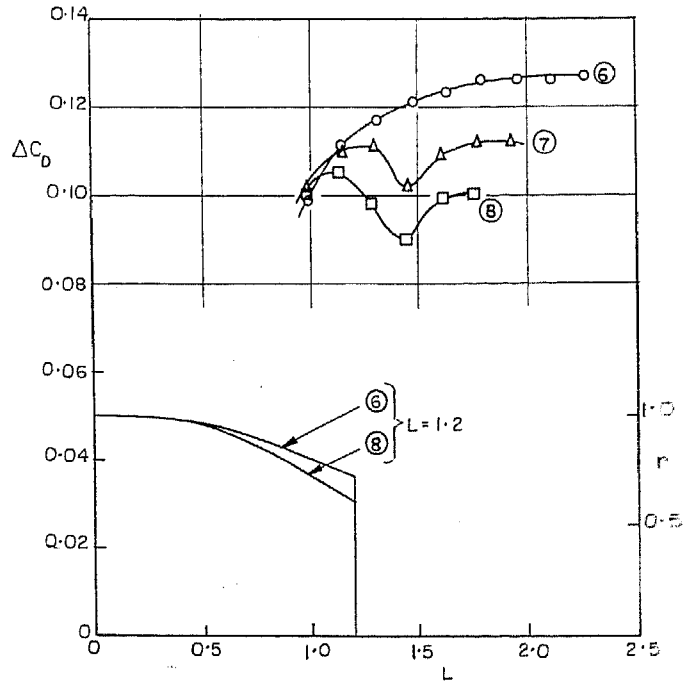

Figure 6. Drag reduction due to boat-tailed afterbodies 6, 7 and 8.

The three afterbodies shown in Fig. 5 were made in this way, with cones of semi-apex angles 22, 26 and 30 degrees. The drag was measured only for afterbody lengths greater than 1, so that for each body the boat-tail angle θ was constant.

The results given in Fig. 6 show that for $L \simeq 1$ the drag reduction is about the same for each of the three bodies 6, 7 and 8, but for greater lengths body 6 is clearly the best. It is remarkable that for $L > 1{\cdot}4$ body 6 gives a greater reduction of drag than either of the conventional fairings shown in Fig. 2. The minimum of ΔC_D occurring for $L = 1{\cdot}45$ with bodies 7 and 8 was associated with unsteady flow, as already discussed in connection with body 3.

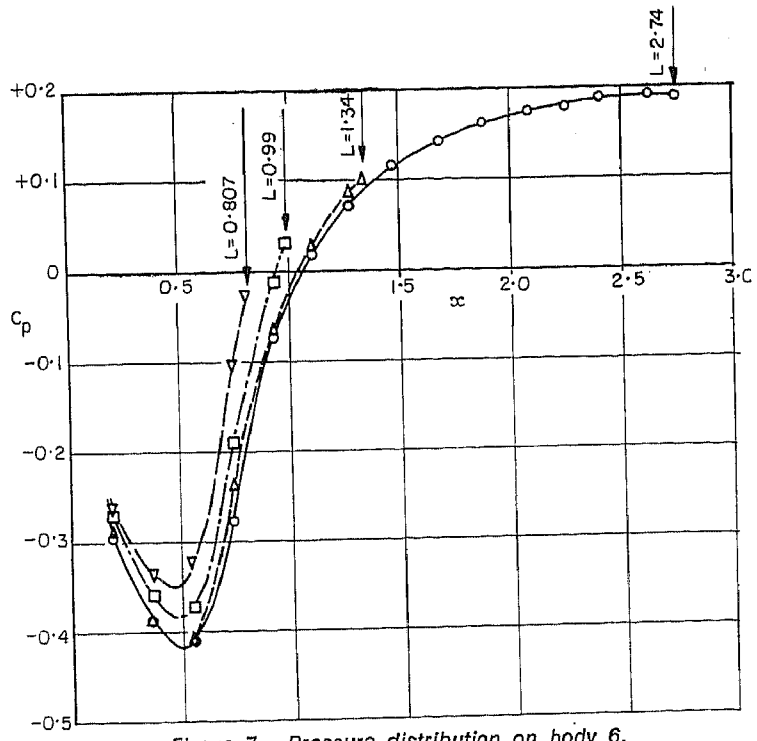

Figure 7. Pressure distribution on body 6.

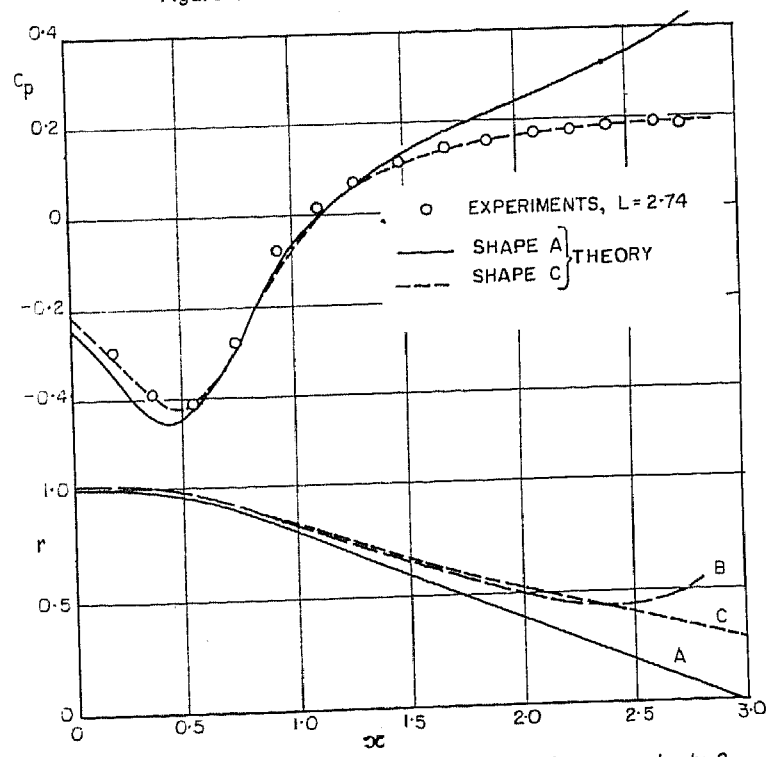

Figure 8. Pressure distributions and boundary layers on body 6.

A Body with no boundary layer.
B Boundary layer displacement surface calculated by Head's method[7].
C Displacement surface assumed for computation of pressure distribution.

Figure 6 suggests that it may be possible for attached flow to persist as far as a cut-off base at $L \simeq 1$ even for a boat-tail angle as large as 30 degrees. However, the drag reduction is then no greater than is obtained with smaller boat-tail angles (22 or 26 degrees) and with increase of L above about 1·3 separation does probably occur ahead of the base unless the boat-tail angle is as small as 22 degrees.

3. Pressure Distributions

An additional model of body 6 was made and fitted with 15 surface pressure holes, arranged in a row along the bottom of the model so that they were removed as far as possible from any influence of the wakes from the model supports. The model was made of Perspex with an initial length L of 2·74 and the pressure distribution was measured for this length and again for a number of smaller lengths by progressively cutting off the base. The holes drilled inside the model were arranged so that as the model was shortened additional holes appeared in the base to replace those at the bottom of the model which had been cut off.

Figure 7 shows the pressure distributions on body 6 for four different lengths. In each case the point indicated by the vertical arrow refers to the edge of the base. There was no appreciable variation of pressure across the base for $L > 1{\cdot}3$, but for smaller lengths the mean value of C_{pB} was about 0·005 less than the value at the edge.

A striking feature of Fig. 7 is the near coincidence of the curves for L greater than about 1, indicating that the effect on the upstream pressure distribution of the recirculating region behind the base is closely similar to that of the complete conical body.

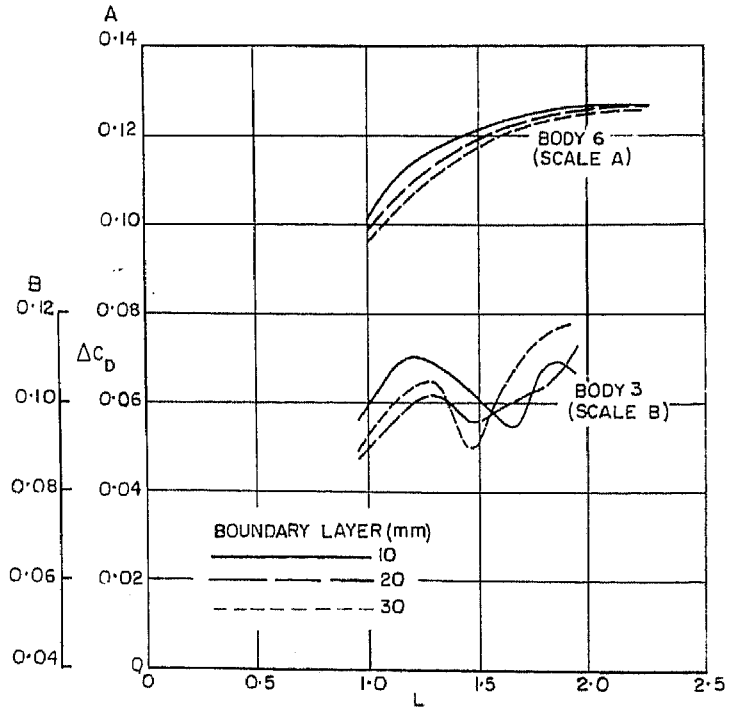

Figure 9. Drag reduction due to afterbodies 3 and 6 with thickened boundary layers.

Figure 7 indicates the type of pressure distribution that is required for a boat-tailed afterbody to give a large reduction of drag for a short length. Much of the total recovery of pressure occurs as a steep rise while x is still fairly small, yet the rise of pressure is not sufficient to cause separation.

The influence of the boundary layer was expected to be large towards the rear of the afterbody and, to throw some light on this, some computations were made for inviscid flow, using the computer program developed by Hess and Smith[6]. The full line in the upper part of Fig. 8 shows the computed pressure distribution for body 6 with no allowance for the boundary layer. Comparison of this curve with the experimental points shows a large effect of the boundary layer for $x > 1{\cdot}6$, suggesting the possibility of separation towards the rear of the body.

Using the measured pressure distribution, the development of the boundary layer was calculated by Head's entrainment method[7], with the entrainment and momentum equations adapted to axisymmetric flow. The boundary-layer radius in these equations was taken to be equal to the body radius, so that the calculation was only valid when the boundary-layer thickness was small compared with the body radius. Curve B at the bottom of Fig. 8 shows the body shape modified by the calculated displacement thickness; the rapid increase of r for $x > 2{\cdot}4$ is caused by the invalid assumption when the body radius is small and should be disregarded.

Using the curve B as a guide, but ignoring the part for $x > 2{\cdot}4$, an attempt was made to sketch a more realistic effective body shape. A further computation of pressure distribution was made for this body shape and the result was used to sketch a still better approximation to the effective body shape. This is shown as curve C at the bottom of Fig. 8 and the computed pressure distribution for this shape is shown to agree well with the measured pressure distribution. Thus curve C at the bottom of Fig. 8 must represent the true effective body shape fairly closely. The fair agreement between the effective body shapes B and C for $x < 2{\cdot}4$ suggests that the boundary layer probably did not separate for $x < 2{\cdot}7$ and that the large effect of the boundary layer on the pressure distribution for $x > 1{\cdot}6$ was caused only by the increase of boundary-layer thickness.

4. Measurements with Thickened Boundary Layers

The effects of thickening the boundary layer on the body were all fairly small and only a few typical results are given as examples. The boundary-layer thicknesses that are given refer to the position CF as shown in Fig. 1, in the absence of an afterbody.

Figure 9 shows the effect on ΔC_p of thickening the boundary layers on bodies 3 and 6. The small and consistent effect shown for body 6 is typical for a body with no double maximum of ΔC_p. The bodies with a double maximum showed a more complex behaviour, usually of the kind shown for body 3. There were other cases in which a double maximum occurred when the boundary layer was thin but not when it was thick, or vice versa.

The changes of pressure distribution on body 6 caused by increase of boundary-layer thickness were in general fairly small and of the kind shown for $L = 1{\cdot}34$ in

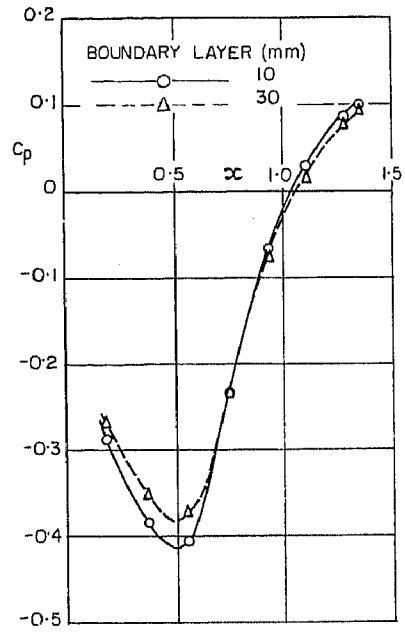

Figure 10. Pressure distribution on body 6 (L=1·34) with different thickness of boundary layer.

Fig. 10. In this case the lower pressure for $x > 0{\cdot}8$ with the thicker boundary layer gives an increase of drag, but this is partly counteracted by the reduced suction in the region of $x=0{\cdot}5$.

5. Components of Afterbody Drag

The components of afterbody drag are related by the equation

$$C_{DB}+C_{Df}+C_{Dc}=0{\cdot}165-\Delta C_D, \tag{1}$$

where C_{DB} is the base drag coefficient, C_{Df} is due to skin friction on the afterbody, C_{Dc} is due to normal pressure on the curved surface of the afterbody and 0·165 is taken to be the value of C_{DB} with no afterbody. For body 6 with various lengths, C_{DB} and ΔC_D are known, and if axial symmetry of the pressure distribution is assumed C_{Dc} can be found by integration. Using this approach the values of C_{Df} found from equation (1) appeared to be unreasonably large and an alternative approach was therefore adopted, as shown in Fig. 11. Curve C shows the value of C_{Df} as calculated by Head's method[7] for the measured pressure distribution. Since C_{Df} is small in comparison with the other drag components a relatively large error in its estimation will be unimportant. Curve B shows C_{DB} as obtained from the measured pressure distribution over the base and curve A is obtained from the direct drag measurements. Curve D is then obtained by subtraction, using equation (1).

The discrepancy now appears in C_{Dc} and for $L > 1$ the values obtained by integration of the measured pressures are about 0·01 below the curve D. One possible explanation for the discrepancy is that the wakes from the model supports at S (Fig. 1) may have reduced the pressure recovery on the afterbody in the region

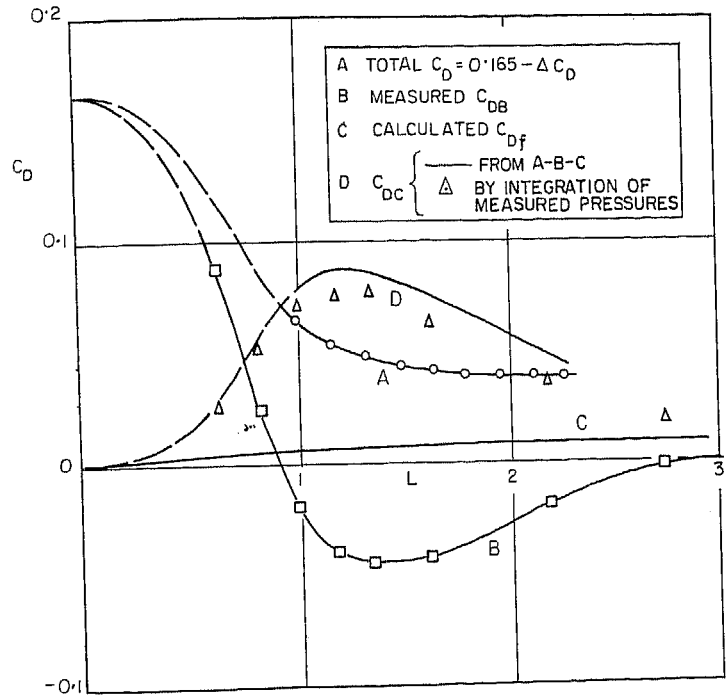

Figure 11. Components of drag coefficient for afterbody 6.

—— —— —— suggested extrapolations to L=0.

of the horizontal plane of symmetry. This would make the measured values of ΔC_D too small for all the afterbodies (including those shown in Fig. 2). A second possibility is that the measurements of ΔC_D were substantially correct but the pressure distributions were not quite axisymmetric, perhaps because of a small inclination of the body to the stream, so that integration of the measured pressure distributions gave values of C_{DC} that were too small. Some support for the second explanation is provided by examination of the pressure distributions shown in Fig. 8. If the experimental pressure distribution for $L=2{\cdot}74$ is modified in the range $0{\cdot}7 < x < 1{\cdot}2$, so that it coincides with the theoretical pressure distribution for shape C, the value of C_{DC} obtained by integration is increased by 0·007. Corresponding modifications of the measured pressure distributions for smaller values of L give increases of C_{DC} of the same order. Thus it seems likely that the *curves* shown in Fig. 11 are all substantially correct, say within $\pm 0{\cdot}005$, and that the points obtained for C_{DC} by integration are too low.

6. Discussion

In previous work on blunt-based boat-tailed bodies much of the emphasis has been on the estimation of base pressure and attempts have often been made to relate this empirically to boat-tail angle and boundary-layer thickness. If only the flow downstream of the base is considered this type of empirical approach seems reasonable, but Fig. 7 suggests that the problem will usually be more

complicated because the pressure distribution on the afterbody ahead of the base is likely to have an important effect on the base pressure. Moreover, the results of Fig. 11 show that C_{Dc} is just as important as C_{Db} in determining the total drag of the afterbody and accurate estimation of C_{Dc} seems at present to be very difficult.

Figure 7 suggests a possible approach to the problem of predicting the drag of a blunt-based boat-tailed afterbody. If the pressure distribution could be calculated for the complete afterbody extending to a pointed tail, with correct allowance for the boundary layer, it might be roughly correct to assume that, for the body cut off at $x=L$, the pressure distribution for $x<L$ would be the same as for the complete body. Unfortunately calculations of drag made on this basis for body 6, using the experimental pressure distribution for $L=2{\cdot}74$, show that no useful quantitative results can be obtained. This is because C_{Dc} is quite strongly influenced by small changes of pressure distribution. As L is reduced from 2·74 the change of pressure distribution is fairly small so long as L is greater than about 1·1, but in this range of L the total drag depends on the difference of two quantities of the same order (curves B and D in Fig. 11), so that errors in C_{Dc} have a large effect. For $L<1{\cdot}1$ the change of pressure distribution becomes larger and this has a large effect on C_{Dc}.

Although quantitative prediction of afterbody drag does not seem to be possible, some progress can be made in specifying qualitatively the essential characteristics of a good boat-tailed afterbody. It will be assumed that the afterbody is at the rear of a long cylindrical body so that the potential flow near the afterbody is not appreciably influenced by the forebody. It is convenient to consider first a complete streamline afterbody with a pointed tail. In inviscid flow this must have zero drag and the positive pressure drag that is found in a real flow is due to reduced pressure recovery at the rear of the body. The reduced pressure recovery is not necessarily associated with separation; it may be due entirely to the thickness of the boundary layer.

When a *two-dimensional* turbulent boundary layer in zero pressure gradient encounters a sudden rise of pressure, the maximum rise of C_p that can occur without separation is known from experiments[8,9] to be about 0·35 to 0·4. The maximum value of C_p that can be reached on an afterbody is expected to be less than this for two reasons. First, in axisymmetric flow with decreasing radius the convergence of the surface streamlines causes more rapid thickening of the boundary layer than in two-dimensional flow. Secondly, in the flow over an afterbody C_p starts near zero, falls rapidly to a minimum and then rises rapidly (Fig. 7). At the point where $C_p=0$ in the region of rapidly rising pressure the boundary layer will already have a rather greater value of the form parameter H than in zero pressure gradient, so that the maximum rise of C_p from this point will be reduced.

It may be concluded that the maximum attainable value of C_p on an afterbody is probably about 0·2 to 0·25. If the afterbody is cut off to form a blunt base before this value is reached, the maximum C_p (at the base) will then be less.

We may now consider the application of these ideas to the design of afterbodies. Taking bodies 2 and 6 as examples of poor and good shapes, Fig. 12 shows the radial distribution of rC_p as computed for inviscid flow by the method

of Ref. 6. For each curve the areas of loops A and B are equal, so that the net drag is zero. C_2 and C_6 are the points on the two curves corresponding to $C_p=0{\cdot}225$. If the real pressure distribution for each body followed the inviscid distribution as far as the point C, and then continued with C_p constant, the pressure drag would be represented by the area of the loop B that is cut off by the straight line from the origin to C. This area is much greater for body 2 than for body 6 and, although the assumed pressure distribution is a crude representation of what may really occur, the argument does perhaps go some way towards explaining why the complete body 2 has a higher drag than body 6.

The same type of argument may be used to indicate qualitatively the probable difference between the bodies when each is cut off to form a blunt base. The point P where the curves intersect is convenient for the purpose of illustration; at that point $C_p=0{\cdot}05$ and $x=1{\cdot}23$ for both bodies. If it is assumed that when each body is cut off at this value of x the pressure distribution is the same as the inviscid one upstream of the base, and that $C_p=0{\cdot}05$ over the base, the pressure drag is given by the area of the loop B that is cut off by the straight line from the origin to P. Again, this is greater for body 2 than for body 6.

These rather crude arguments indicate that for a good afterbody design the area of the complete loop B should be small. Since for inviscid flow the areas of loops A and B must be equal this is equivalent to a requirement that the loop A should be small. Over the part of the body corresponding to loop A the pressure distribution is not likely to be strongly influenced by the boundary layer unless early separation occurs, so that for a qualitative comparison of body shapes it is probably sufficient to consider only the inviscid pressure distributions.

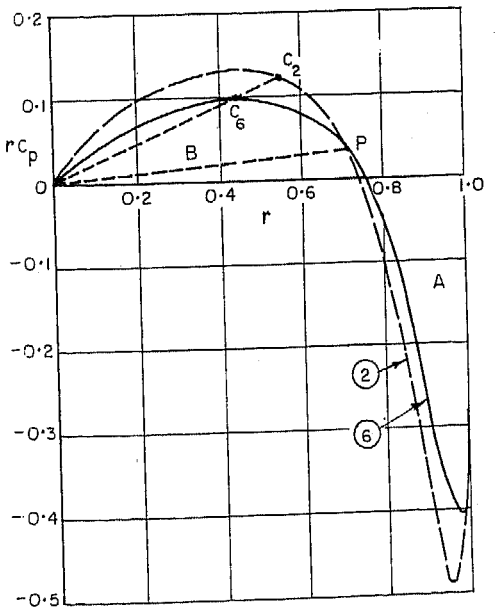

Figure 12. Radial distribution of rC_p for inviscid flow.

The assumptions that have been made will not be even roughly correct if separation occurs ahead of the cut-off base. It should therefore be specified that in shaping the complete body to minimise the area of loop A the pressure distribution should be such that separation does not occur ahead of the proposed cut-off position.

For practical reasons the boat-tailed afterbody may be required to be short. An additional design condition is then that on the complete body C_p should rise to a significant positive value (say 0·1) in the shortest possible distance from the upstream end that is compatible with the other requirements.

7. Conclusions

A substantial reduction of drag has been obtained with an afterbody consisting of a smooth fairing leading to a conical tail-piece of semi-angle 22 deg. At the Reynolds number of these experiments this afterbody, with a length of only 60 per cent of the maximum diameter, gave almost as much reduction of drag as a conventional streamline tail. Changes of boundary-layer thickness had only small effects on the drag reductions obtained with the boat-tailed afterbodies, so that variations of Reynolds number might also be expected to have only small effects. At higher Reynolds numbers the drag reduction obtained with a conventional streamline tail might be greater and such a tail might then compare rather more favourably with the boat-tailed afterbodies.

Acknowledgment

The author is grateful to Mr. D. N. Foster of the Aerodynamics Department, Royal Aircraft Establishment, for computing the pressure distributions shown in Figs. 8 and 12.

References

1. CALVERT, J. R. Blockage corrections for blunt-based bodies of revolution. *Journal of the Royal Aeronautical Society*, Vol. 70, pp 532-533, 1966.
2. MAIR, W. A. Blockage corrections for blunt-based bodies of revolution. *Aeronautical Journal*, Vol. 72, p 1058, 1968.
3. EVANS, J. Y. G. Corrections to velocity for wall constraint in any 10×7 rectangular subsonic wind tunnel. ARC R & M 2662, 1953.
4. LOCK, C. N. H. and JOHANSEN, F. C. Drag and pressure distribution experiments on two pairs of streamline bodies. ARC R & M 1452, 1933.
5. WIEGHARDT, K. Betrachtungen zum Zähigkeitswiderstand von Schiffen. *Jahrbuch der Schiffbautechnischen Gesellschaft*, Vol. 52, pp 184-199, 1958.
6. HESS, J. L. and SMITH, A. M. O. Calculation of potential flow about arbitrary bodies. *Progress in Aeronautical Sciences*, Vol. 8, Pergamon, 1967.
7. HEAD, M. R. Entrainment in the turbulent boundary layer. ARC R & M 3152, 1960.
8. BRADSHAW, P. and GALEA, P. V. Step-induced separation of a turbulent boundary layer in incompressible flow. *Journal of Fluid Mechanics*, Vol. 27, pp 111-130, 1967.
9. HEAD, M. R. and RECHENBERG, I. The Preston tube as a means of measuring skin friction. *Journal of Fluid Mechanics*, Vol. 14, pp 1-17, 1962.